Title

Thermally driven phase transition of halide perovskites revealed by big data-powered in situ electron microscopy

Journal

The Journal of Chemical Physics, 158(13)

ISSN

0021-9606

Authors

Luo, Xin
Liu, Weiyan
Wang, Zeyu
et al.

Publication Date

2023-04-07

DOI

10.1063/5.0144196

Peer reviewed

Thermally driven phase transition of halide perovskites revealed by big data-powered *in situ* electron microscopy

Xin Luo,[1,2] Weiyan Liu,[1] Zeyu Wang,[1,2] Teng Lei,[3] Peidong Yang,[3,4,5,6,a)] and Yi Yu[1,2,a)]

AFFILIATIONS

[1]School of Physical Science and Technology, ShanghaiTech University, Shanghai 201210, China
[2]Shanghai Key Laboratory of High-resolution Electron Microscopy, ShanghaiTech University, Shanghai 201210, China
[3]Department of Chemistry, University of California Berkeley, Berkeley, California 94720, USA
[4]Materials Sciences Division, Lawrence Berkeley National Laboratory, Berkeley, California 94720, USA
[5]Department of Materials Science and Engineering, University of California Berkeley, Berkeley, California 94720, USA
[6]Kavli Energy NanoScience Institute, Berkeley, California 94720, USA

Note: This paper is part of the JCP Special Topic on 40 Years of Colloidal Nanocrystals in JCP.
[a)]Authors to whom correspondence should be addressed: p_yang@berkeley.edu and yuyi1@shanghaitech.edu.cn

ABSTRACT

Halide perovskites are promising light-absorbing materials for high-efficiency solar cells, while the crystalline phase of halide perovskites may influence the device's efficiency and stability. In this work, we investigated the thermally driven phase transition of perovskite ($CsPbI_xBr_{3-x}$), which was confirmed by electron diffraction and high-resolution transmission electron microscopy results. $CsPbI_xBr_{3-x}$ transitioned from δ phase to α phase when heated, and the γ phase was obtained when the sample was cooled down. The γ phase was stable as long as it was isolated from humidity and air. A template matching-based data analysis method enabled visualization of the thermally driven phase evolution of perovskite during heating. We also proposed a possible atomic movement in the process of phase transition based on our *in situ* heating experimental data. The results presented here may improve our understanding of the thermally driven phase transition of perovskite as well as provide a protocol for big-data analysis of *in situ* experiments.

I. INTRODUCTION

Halide perovskites are promising optoelectronic materials due to their solution-processability and are heavily researched for solar cell applications with high power conversion efficiencies.[1–4] Halide perovskites undergo phase transition induced by heating and other environmental stimuli, which can influence their photovoltaic performance.[5,6] Taking $CsPbI_3$ as an example, the classic cubic perovskite structure (α phase) is unstable at ambient conditions due to thermodynamic instability.[7,8] α-$CsPbI_3$ spontaneously lowers its symmetry and then transforms to a non-perovskite structure (δ phase) with double chains of Pb–I octahedra under humid conditions.[9,10] Moreover, the cubic perovskite structure can be undercooled below its transition temperature and maintain its perovskite phase down to room temperature at the expense of twists of Pb–I octahedra (γ phase).[8,11] Thus far, the mechanism of the thermally driven phase evolution has not been clearly explained at the atomic level. Since differences in lattice volume and the arrangement of Pb–I octahedra between the α phase and δ phase are significantly large,[12] it is rather interesting to study time-resolved thermally driven phase evolution. In traditional experiments, x-ray diffraction (XRD) is usually used to confirm the phase of the bulk perovskite before and after the phase evolution, whereas nanoscale detailed structural information during phase evolution is missing. Therefore, a characterization method with a high spatial and temporal resolution is needed. *In situ* transmission electron microscopy (*in situ* TEM) can provide *in situ* heating capability, and the nanoscale structural evolution of halide perovskites could be tracked by using a fast camera.

However, it has been challenging to carry out *in situ* heating TEM experiments for halide perovskites so far. On one hand, halide perovskites are beam-sensitive,[13,14] which means that prolonged

high-resolution TEM (HRTEM) imaging would cause serious structural damage to the sample. On the other hand, $CsPbI_3$ converts to cubic structure (α phase) at a rather high temperature (~320 °C), and therefore heating and imaging at high temperature would cause decomposition of $CsPbI_3$ under the combined influence of electron beam irradiation and heat, hindering the observation of phase transition. To address these two issues, here, we come up with the following solutions. Instead of imaging, by using selected-area electron diffraction (SAED), the phase of halide perovskite can be confirmed and the time-resolved thermally driven phase evolution can be investigated under relatively low electron doses, avoiding the beam-induced structural damage. Furthermore, lowering the phase transition temperature of halide perovskite is possible through alloying. For example, by doping with Br element, the alloyed $CsPbI_xBr_{3-x}$ ($x \leq 1$) has a similar structure with $CsPbI_3$ but a lower phase transition temperature could be obtained. This has been confirmed by cathodoluminescence microscopy.[15] Utilizing the micro-analysis capability of TEM,[14,16,17] here, the thermally driven evolutions of the three phases of $CsPbI_xBr_{3-x}$ were directly observed and recorded *in situ*.

The next question is related to the large datasets generated during the *in situ* heating experiments. How to analyze large datasets effectively and efficiently is becoming a matter of concern. Numerous efforts have aimed to solve this problem by taking advantage of deep learning,[18,19] image processing technology,[20] and so on. In this work, a single *in situ* diffraction video contains thousands of diffraction patterns detailing the temporal information of the thermally driven phase evolution process. The conventional manual method analyzes diffraction patterns individually, which is highly time-consuming, and erroneous judgments may occur when the amount of data is large. Here, by developing an automatic diffraction analysis method based on dimension reduction and template matching, the changes in the diffraction patterns of the phases can be revealed based on objective criteria, and consequentially artificial errors could be avoided. Based on these analysis results, a possible atomic displacement model for the phase transition is proposed, which may be constructive to understanding the thermally driven phase transition.

II. RESULTS AND DISCUSSION

A. Workflow of *in situ* TEM experiments

For *in situ* heating, an E-chip with a silicon nitride membrane film was applied to hold the sample, instead of a traditional TEM grid. A schematic of the E-chip is shown in Fig. 1(a). The $CsPbI_xBr_{3-x}$ nanowires were transferred from the glass substrate, dispersed in isopropanol, and then drop-casted on the E-chips. Similar to the pure components $CsPbI_3$ and $CsPbBr_3$, $CsPbI_xBr_{3-x}$ nanowires undergo thermally driven phase transition, as shown in Fig. 1(b). δ-$CsPbI_xBr_{3-x}$ with non-perovskite phase is stable at room temperature, and it will transform to α-$CsPbI_xBr_{3-x}$ with cubic perovskite phase upon heating. Moreover, a tetragonal perovskite phase β-$CsPbI_xBr_{3-x}$ and an orthorhombic perovskite phase γ-$CsPbI_xBr_{3-x}$ can be obtained in sequence after the temperature is reduced to room temperature. α-$CsPbI_xBr_{3-x}$ has a classical cubic perovskite structure, while β-$CsPbI_xBr_{3-x}$ and γ-$CsPbI_xBr_{3-x}$ are generated by unique characteristic distortions in Pb–X octahedra. Figure 1(c) summarizes the brief process of the whole experiment.

The temperature treatment of the $CsPbI_xBr_{3-x}$ nanowires was controlled by an *in situ* heating holder with a ramp rate of 0.5 °C/s, and the temperature was kept at 170 °C for about 70 min. In the cooling process, the sample was directly cooled down from 170 °C to room temperature within 1 s, after which the E-chip was stored in a glove box. The temperature of 170 °C is chosen because the thermally driven phase transition can occur at this temperature and the nanowires will not be thermally decomposed. SAED of the nanowire indicated that the phase of $CsPbI_xBr_{3-x}$ nanowires changed during the process so that it can be utilized to investigate the phase evolution. By capture of large quantities of SAED patterns with high temporal resolution, an *in situ* diffraction movie can be obtained. Utilizing the template matching-based analysis method that we have developed, structural evolution was revealed and discussed here in detail.

B. Phase confirmation by low dose HRTEM

A typical electron dose for HRTEM imaging is about 10^4–10^5 e/Å^2. In order to prevent the electron beam damage, low electron doses, about 800 e/Å^2, were used when recording HRTEM. Wiener filtering was applied to HRTEM images in order to improve the signal-to-noise ratio and obtain high-quality images. Figure 2(a) shows the initial morphology of a $CsPbI_xBr_{3-x}$ nanowire on the silicon nitride membrane of the E-chip. The corresponding HRTEM images and Fourier transform patterns are displayed in Fig. 2(b). The Fourier transform pattern was indexed to be δ-$CsPbI_xBr_{3-x}$ in [001] zone axis, confirming the $CsPbI_xBr_{3-x}$ nanowire was initially δ phase. δ-$CsPbI_xBr_{3-x}$ shows the spacings of 3.3 Å for the (120) and the (120) lattice planes [Fig. 2(b)]. Here, the index of $CsPbI_xBr_{3-x}$ was referred to the crystal structure of δ-$CsPbBr_3$, as has been done in previous reports.[15] Figure 2(c) shows the morphology of the $CsPbI_xBr_{3-x}$ nanowire after phase transition when the temperature has reached 170 °C and been maintained for some time. The HRTEM and its Fourier transform pattern are shown in Fig. 2(d). Here, the nanowire has been tilted to a low-index zone axis before HRTEM. Compared with the Fourier transform in Fig. 2(b), the change of pattern indicates that the phase of this region has changed. The Fourier transform in Fig. 2(d) was indexed to be α-$CsPbI_xBr_{3-x}$ in [111] zone axis. The lattice fringes of α-$CsPbI_xBr_{3-x}$ have interplanar spacings of 4.2 Å, matched well, respectively, with those of the (110) and the (101) planes. The measured interplanar spacings for $CsPbI_xBr_{3-x}$ have deviations of ~0.1 Å from standard $CsPbBr_3$, and minor changes of lattice parameters are attributed to the doping of I atoms in $CsPbI_xBr_{3-x}$.

Next, the thermally driven phase transition from α-$CsPbI_xBr_{3-x}$ to γ-$CsPbI_xBr_{3-x}$ induced by cooling was also confirmed by HRTEM. The nanowires were directly cooled from 170 °C to room temperature rapidly, which was similar to the quenching process in preparing γ-$CsPbI_xBr_{3-x}$ nanowire samples.[11] Notably, due to the rapid cooling rate, the β-$CsPbI_xBr_{3-x}$ in the cooling process is difficult to be observed. The γ phase was stable at room temperature, and it could be confirmed by checking the E-chip after the *in situ* experiments. The E-chip was stored in the glove box filled with argon to protect the specimen from being exposed to humidity and oxygen. γ-$CsPbI_xBr_{3-x}$ phase was still preserved when checking the HRTEM afterward.

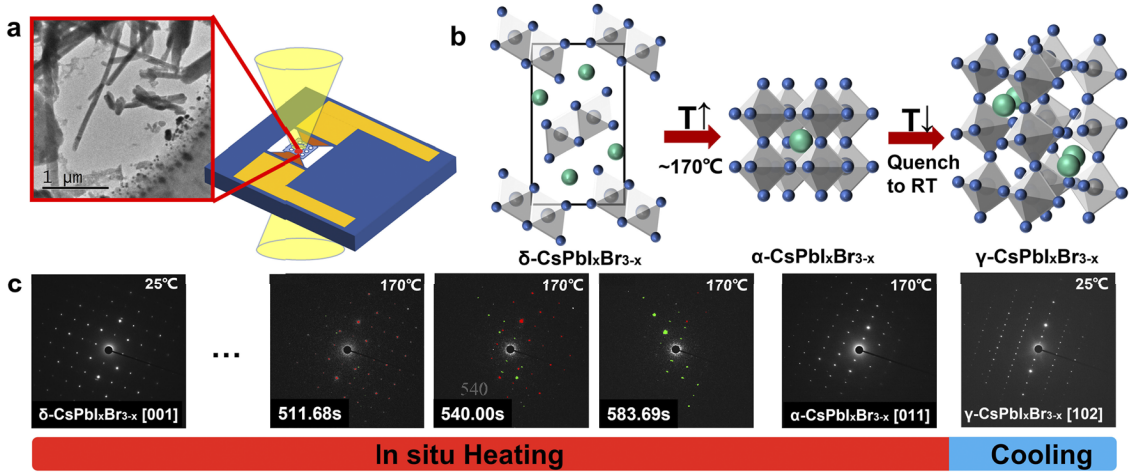

FIG. 1. Schematics of the experiments. (a) Schematic of *in situ* heating E-chip. (b) Schematics of the δ-$CsPbI_xBr_{3-x}$, α-$CsPbI_xBr_{3-x}$ and γ-$CsPbI_xBr_{3-x}$ crystal structures. (c) The evolution of *in situ* SAED patterns that represent the phase evolution of nanowires in real time.

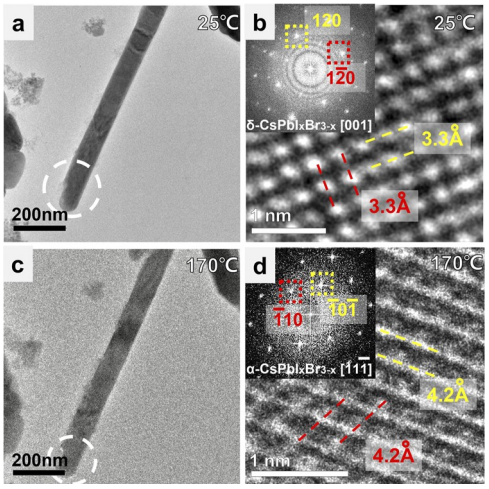

FIG. 2. Phase transition confirmed by HRTEM. (a) Morphology of a $CsPbI_xBr_{3-x}$ nanowire at room temperature. (b) Corresponding HRTEM and Fourier transform pattern of the region marked by a white circle in (a). (c) Morphology of the $CsPbI_xBr_{3-x}$ nanowire at 170 °C. (d) Corresponding HRTEM and Fourier transform pattern of the region marked by white circle in (c). Low-dose HRTEM images are processed by a Wiener filter to achieve a higher signal-to-noise ratio.

Figure 3(a) shows the morphology of the $CsPbI_xBr_{3-x}$ nanowire observed in Fig. 2(c) after cooling. The corresponding SAED and HRTEM are shown in Figs. 3(b) and 3(c), where single-crystalline feature can still be seen. The diffraction [Fig. 3(b)] is different from that of α-$CsPbI_xBr_{3-x}$, indicating phase transition has occurred. The diffraction pattern is indexed to be γ-$CsPbI_xBr_{3-x}$ in [102] zone axis, suggesting that the $CsPbI_xBr_{3-x}$ nanowire converts to γ phase after cooling and being well preserved. HRTEM in Fig. 3(c) shows the (040) lattice planes of $CsPbI_xBr_{3-x}$ nanowires, which is 2.9 Å. Lattice planes perpendicular to the (040) plane have a larger spacing in the reciprocal space, which means a smaller spacing in real space and is difficult to be distinguished. The thermally driven phase transition of another nanowire (Fig. S1) reproduces the evolution among δ, α, and γ phases, confirming the generality of the results in Figs. 2 and 3. Moreover, the nanowire in Fig. S1 was not continuously exposed to the electron beam during *in situ* heating experiment, indicating that electron beam-induced effects had little influence on the phase evolution of $CsPbI_xBr_{3-x}$ nanowires, and thermal heat from the E-chip plays a major role. To compare with the cooled samples stored in the glove box, in another experiment, the cooled nanowire was characterized once obtained (Fig. S2) and was indexed to be γ-$CsPbI_xBr_{3-x}$, indicating that γ-$CsPbI_xBr_{3-x}$ was formed as soon as the temperature dropped. Therefore, it can be concluded that the as-obtained γ-$CsPbI_xBr_{3-x}$ phase is more stable at room temperature in the inert environment than halide perovskite in a humid environment.[9,21] Thus far, the observation of thermally driven phase transition of $CsPbI_xBr_{3-x}$ perovskite nanowires from the δ phase to α phase and from the α phase to γ phase has been confirmed in TEM, making use of *in situ* heating chips. Since the *ex situ* HRTEM provides only the snapshot results and the time-resolved information of the evolution process is missing, the next question is how these crystalline phases evolve in real-time. As mentioned before, in order to avoid serious beam damage to the nanowires under the prolonged *in situ* HRTEM exposure, in the following, the thermally driven phase evolution was revealed by recording and analyzing SAED patterns at lower magnifications and much lower dose rates.

C. Phase evolution revealed by *in situ* electron diffraction

The thermally driven phase evolution was monitored by recording *in situ* SAED patterns, whereas a typical *in situ* SAED movie (Movies S1–S3) contains ~12 000 frames, which means that the dataset can hardly be analyzed manually. In addition, subtle differences in SAED movies during phase evolution are also difficult to be distinguished manually. Therefore, a template matching-based[20]

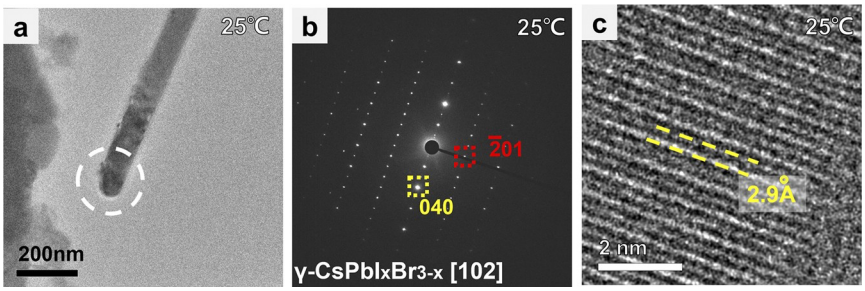

FIG. 3. Phase transition induced by cooling. (a) Morphology of the $CsPbI_xBr_{3-x}$ nanowire after cooling and being stored in the glove box for a month. (b) SAED of the region marked by a white circle in (a). (c) Corresponding HRTEM image. HRTEM is processed by a Wiener filter to achieve a higher signal-to-noise ratio.

diffraction big-data analysis method combined with data dimension reduction was utilized to solve this problem, and the schematic is shown in Fig. 4.

The whole process of the template matching method can be divided into three steps: template generation, template refinement, and template matching. As shown in Fig. 4(a), principal components analysis (PCA) was introduced to perform data dimension reduction. This is similar to that in face recognition technology, where PCA is applied to get a series of so-called eigenfaces, and then any face can be obtained by a combination of several eigenfaces. In the same way, this data dimension reduction method was applied to analyze *in situ* SAED movies. To generate templates, mini-batches were extracted from the whole dataset and applied with PCA. Since the heating reaction only contained δ-$CsPbI_xBr_{3-x}$ and α-$CsPbI_xBr_{3-x}$, two main principal components, i.e., eigen-patterns, represent these two phases after PCA [Fig. 4(a)]. After that, the initial templates are obtained [in the right of Fig. 4(a)] by applying an intensity mask to the eigen-patterns. The details of eigen-patterns and the weight of the two main principal components over time are shown in Figs. S3 and S4. Since PCA is a mathematical data analysis method, the physical meaning of initial templates extracted from PCA results needs to be revealed and errors need to be eliminated. Based on the partial rotation average of standard diffraction patterns applied to the initial templates, the identification of phases was achieved [Fig. 4(b)]. To be noted that, there are a few weak diffraction spots (2–3 spots) in the pattern, which do not belong to either one of the two phases,

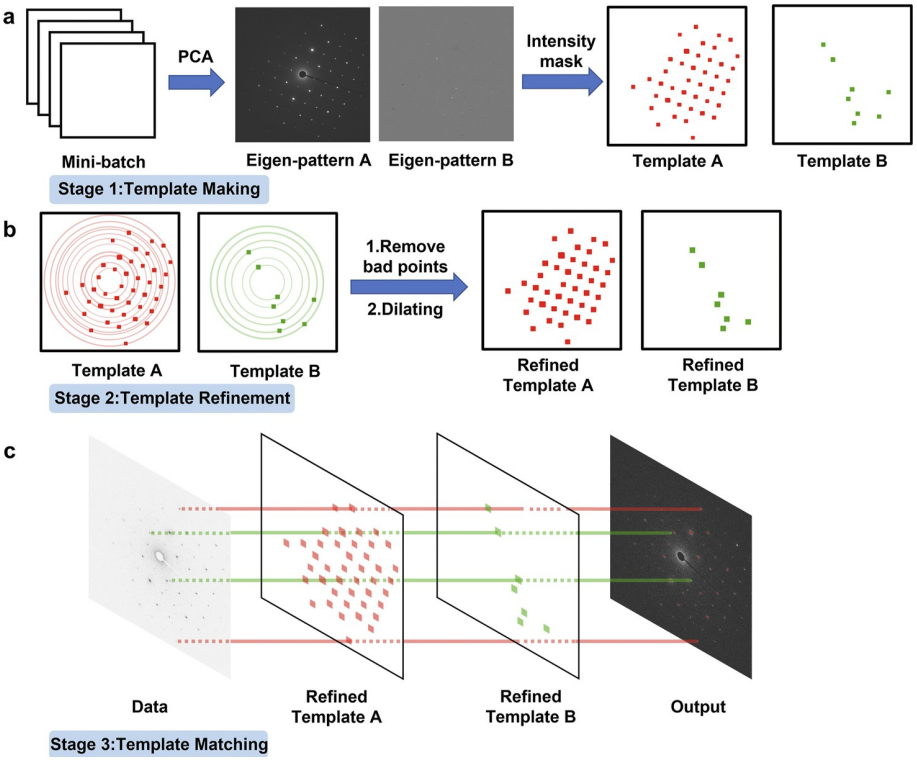

FIG. 4. Schematic of the template matching method for big-data analysis. (a) Generation of the initial templates. (b) Refinement of the initial templates with partial rotation average and dilating. (c) Matching the data with the refined templates.

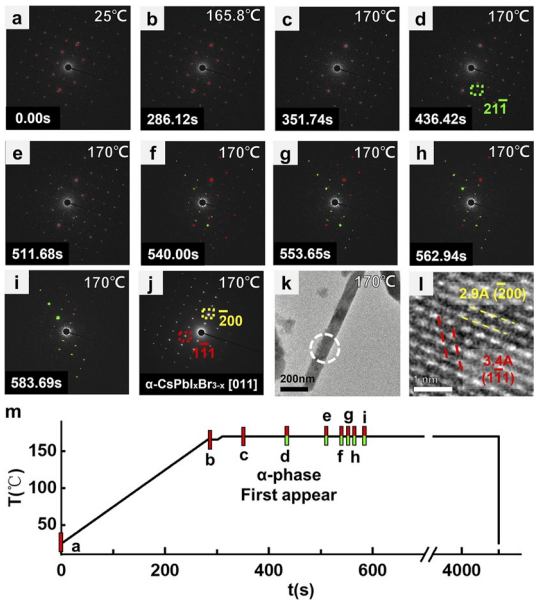

FIG. 5. *In situ* diffraction revealing phase transition. Snapshots from the diffraction movie at (a) 0 s, (b) 286.12 s, (c) 351.74 s, (d) 436.21 s, (e) 511.68 s, (f) 540.00 s, (g) 553.65 s, (h) 562.94 s, and (i) 583.69 s. Spots from different phases are labeled in colors (red represents δ-$CsPbI_xBr_{3-x}$, and green represents α-$CsPbI_xBr_{3-x}$). (j) SAED acquired after specimen tilting. (k) TEM morphology of the α-$CsPbI_xBr_{3-x}$ nanowire after heating. (l) Corresponding HRTEM image. (m) Temperature vs time. Phase evolution data points in (a–i) are marked by sticks in different colors (red represents the appearance of δ-$CsPbI_xBr_{3-x}$, and green represents the appearance of α-$CsPbI_xBr_{3-x}$).

and they are defined as secondary spots. These secondary spots were removed and will not be involved in the following analysis. The origin of these secondary spots may come from the impurities on the nanowire surface or tiny impurity particles that have been included inside the selected-area aperture [as can be seen in Fig. 5(k) in the following]. After that, the templates were dilated for better matching accuracy in the next step (see the supplementary material for details). In the next stage [Fig. 4(c)], the SAED patterns were compared to the refined templates and different phases were labeled by different colors. Once the templates have been refined, the SAED patterns in each frame are labeled by using the template matching method, and labeled diffraction spots of each phase are shown in the same color as the refined template. This operation is repeated automatically until the whole datasets are processed, and hence the efficacy of the template matching method is far greater than manual analysis.

The corresponding analysis result of the SAED patterns in *in situ* heating experiments (Movies S1–S3) is shown in Fig. 5. Two templates representing δ-$CsPbI_xBr_{3-x}$ and α-$CsPbI_xBr_{3-x}$ are used in the analysis, and corresponding diffraction spots are marked in red and green, respectively. Nine representative SAED patterns are shown in Figs. 5(a)–5(i), and the temperature control for $CsPbI_xBr_{3-x}$ nanowires heating up to 170 °C at a ramp rate of 0.5 °C/s is provided in Fig. 5(m). In the initial state [Fig. 5(a)], only the diffraction spots from δ-$CsPbI_xBr_{3-x}$ were found. The corresponding diffraction pattern was indexed to be δ-$CsPbI_xBr_{3-x}$ in the [001] zone axis. Comparing the initial state [Fig. 5(a)] with the first snapshot when the temperature reaches 165.8 °C [Fig. 5(b)], there was no obvious change in the diffraction pattern during the heating process, indicating that $CsPbI_xBr_{3-x}$ remained in δ phase. After reaching 170 °C, the diffraction spots of α-$CsPbI_xBr_{3-x}$ appeared at 436.42 s [Figs. 5(c) and 5(d)], which were indicated by green square in corresponding color, matched well with (211) planes of α-$CsPbI_xBr_{3-x}$, and more and more α-spots appeared over time [Fig. 5(e)]. Meanwhile, the diffraction spots of δ-$CsPbI_xBr_{3-x}$ labeled in red gradually vanished and SAED patterns were dominated by diffraction spots of α-$CsPbI_xBr_{3-x}$ labeled in green [Figs. 5(f)–5(i)]. It could be seen from Fig. 5(i) that the diffraction pattern deviated from the low-index zone axis, so we tilted the specimen back to zone axis for better confirmation after the diffraction pattern was stable and unchanged [Fig. 5(j)]. The SAED pattern was indexed to be α-$CsPbI_xBr_{3-x}$ in the [011] zone axis. Figures 5(k) and 5(l) show the morphology and HRTEM of the nanowire after phase transition, and the white circle represents the aperture area where *in situ* SAED patterns were acquired. The α-$CsPbI_xBr_{3-x}$ shows the spacings of 2.9 and 3.4 Å for the (200) and the (111) lattice planes, respectively. Phase evolution data points in Figs. 5(a)–5(i) were marked by sticks in different colors in Fig. 5(m), which represent the appearance of δ-$CsPbI_xBr_{3-x}$ (red) and α-$CsPbI_xBr_{3-x}$ (green). The delay between reaching 170 °C and the onset of the phase transition may cause by poor thermal diffusivity of the sample or the non-uniform heating of the sample cell. The entire phase evolution was rapid, changing from a diffraction pattern of δ-$CsPbI_xBr_{3-x}$ to a diffraction pattern dominated by α-$CsPbI_xBr_{3-x}$ in about 150 s.

D. A possible atomic movement trajectory proposed based on TEM observations

For the thermally driven phase transition, δ-$CsPbI_xBr_{3-x}$ converts to α-$CsPbI_xBr_{3-x}$ with a 7% increase in volume and atom rearrangement,[12] and therefore it is interesting to understand how the atoms move and re-arrange during the phase transition. Based on the *in situ* SAED movies, the initial state (δ-$CsPbI_xBr_{3-x}$ in the [001] zone axis) and final state (α-$CsPbI_xBr_{3-x}$ in the [011] zone axis) can be confirmed, which provides a basic framework for discussing the atomic motion during the transition from the initial to final state. The three-viewing drawing of δ-$CsPbI_xBr_{3-x}$ and α-$CsPbI_xBr_{3-x}$ is shown in Fig. 6(a), and two top views of lattice are δ-$CsPbI_xBr_{3-x}$ in the [001] zone axis and α-$CsPbI_xBr_{3-x}$ in the [011] zone axis. It can be seen from the three-viewing drawing that the two lattices are very different in the structure of the Pb–X octahedra. For δ-$CsPbI_xBr_{3-x}$, the Pb–X octahedra, which are indicated by green rectangles, are edge sharing, forming a special double chain structure; On the contrary, the Pb–X octahedra in α-$CsPbI_xBr_{3-x}$ are corner sharing, which is the classical perovskite structure. Therefore, the double-chained Pb–X octahedra structure was extracted and analyzed specifically.

Figures 6(b)–6(e) demonstrates the possible trajectory of the atomic movements of the double chain structure during the thermally driven phase evolution. A 3 × 1 × 1 supercell of double-chained Pb–X octahedra is generated in order to better show the atomic movements. In Fig. 6(b), the initial stage of double-chained Pb–X octahedra is shown, and parts of the Pb–X bonds are marked in red. These bonds could first be cleaved by heating. On one hand,

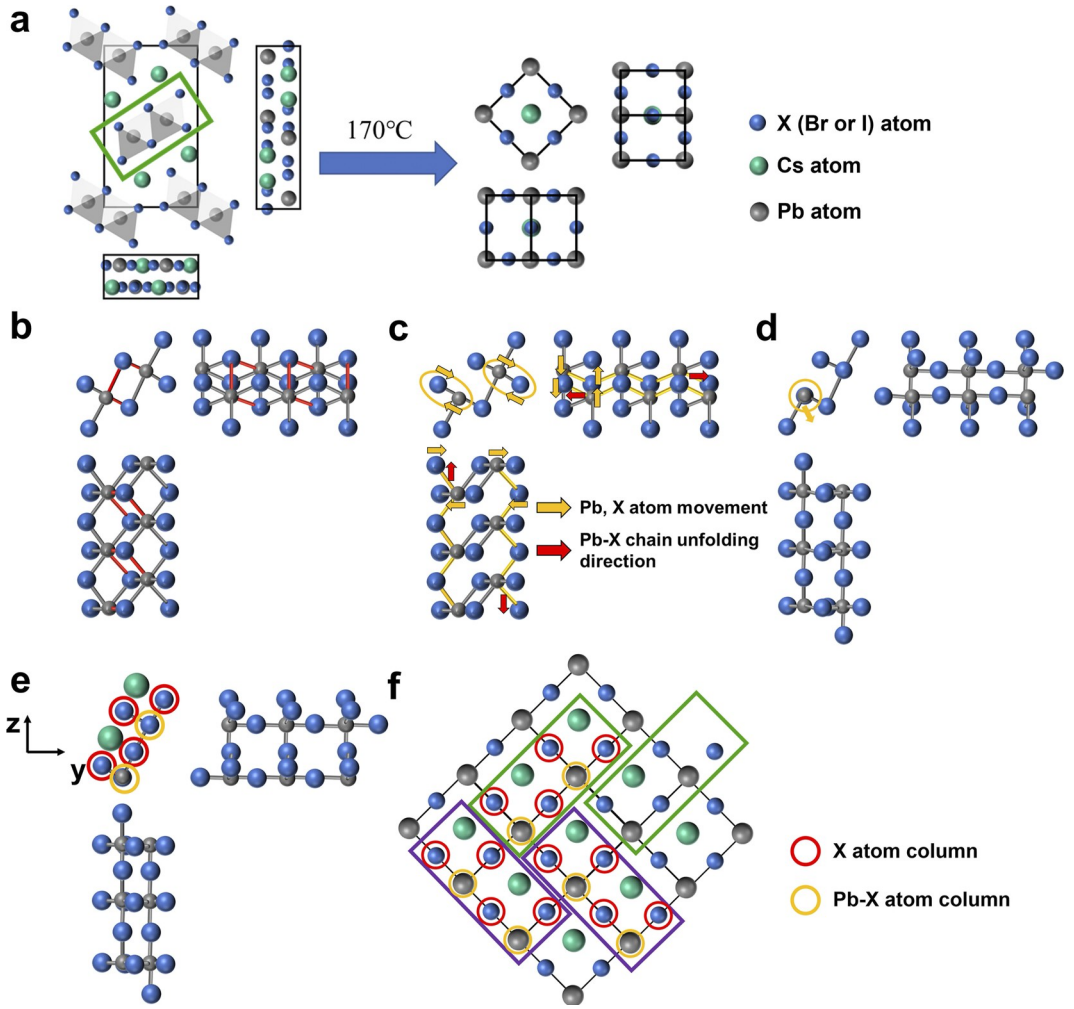

FIG. 6. The proposed atomic movements for phase transition (a) Three-viewing drawing of δ-$CsPbI_xBr_{3-x}$, α-$CsPbI_xBr_{3-x}$. (b) Three-viewing drawing of edge sharing Pb–X octahedra in δ-$CsPbI_xBr_{3-x}$. Broken bonds are marked in red. (c) Unfolding of Pb–X chains and generation of Pb–X atom columns. (d) Position adjustment of Pb–X atom columns (e) Final result leading to corner sharing Pb–X octahedra in α-$CsPbI_xBr_{3-x}$ (f) Reconstruction of α-$CsPbI_xBr_{3-x}$ with the proposed atomic movements.

this bonding cleaving enables the freedom of atomic movement and the next unfolding steps. On the other hand, two closest Pb atoms are linked by two Pb–X–Pb bonds in double-chained Pb–X octahedra, whereas there is only one Pb–X–Pb bond between two closest Pb atoms in α-$CsPbI_xBr_{3-x}$; hence, parts of the Pb–X bonds are proposed to be cleaved in order to match the structure of the α phase.

After this initial bond breaking, the next step is the generation of Pb–X atom columns [Fig. 6(c)]. The corresponding Pb and X atom movements are marked in yellow arrows, and the zigzag distribution of Pb–X atoms chain, which is marked in yellow bonds, can become Pb–X atom columns in classic perovskite structure by simply unfolding, leading to the increase in volume. Moreover, the Pb atoms in the two Pb–X columns are not on the same horizontal position. Therefore, the two columns of atoms need to shift as shown by the red arrows to align the Pb and X atoms during the unfolding process. As shown in the left view, the same operation is performed, which aligns the other direction of the atom columns in the three-dimensional space. It is noteworthy that the proposed generation of Pb–X atom columns could be the most likely way as other possible trajectories may have higher energy barriers. Apart from the chosen X atoms as proposed, another X atom columns linked laterally to Pb atoms can be excluded because there must be a X atom column between the two Pb–X atom columns in the α phase. Moreover, for X atom columns linked vertically to Pb atoms, as the X and Pb atoms are on the same plane, it is quite difficult to generate a Pb–X atomic column due to the steric hindrance effect. Therefore, the Pb–X atomic column is more likely to be obtained from the unfolding of Pb–X chains as marked in yellow circles.

The next step is to adjust the relative position of the X atom columns and Pb–X atom columns [Fig. 6(d)]. In the standard perovskite structure, two closest Pb–X columns are on the edges of the lattice and in a straight line, but two Pb–X columns in the front view do not meet this condition. Hence, the Pb–X columns marked by yellow circles need to move along the yellow arrow; meanwhile, X atom columns and Pb–X atom columns should adjust the position in order to make the lattice constant match that of α-$CsPbI_xBr_{3-x}$. The final result of the double-chained Pb–X octahedra after these atomic movements is shown in Fig. 6(e), which forms an α-$CsPbI_xBr_{3-x}$ fundamental unit as marked in green rectangles in Fig. 6(f). Another series of double-chained Pb–X octahedra are axisymmetric to the structure in Fig. 6(b) before the phase evolution. Therefore, the structure after the phase transition should also be axisymmetric to the final result in Fig. 6(e), which is marked in purple rectangles in Fig. 6(f). Through the combination of the two structures marked in green and purple, the complete α-$CsPbI_xBr_{3-x}$ structure is obtained. The movement of Cs atoms could be much easier than Pb–X octahedra. The Cs atoms only need to adjust the position in the three-dimensional space and enter the gap of the structure in Fig. 6(e). Overall, the proposed atomic movements successfully reconstructed the phase evolution process based on the experimental *in situ* SAED results. However, it should be noted that a rigorous model for structure evolution requires further support from direct atomic-scale imaging and theoretical simulations, which deserves future investigations.

III. CONCLUSIONS

In summary, the thermally driven phase transition of $CsPbI_xBr_{3-x}$ was studied *in situ* inside the TEM. δ-$CsPbI_xBr_{3-x}$ converts to α-$CsPbI_xBr_{3-x}$ after heating, while α-$CsPbI_xBr_{3-x}$ converts to γ-$CsPbI_xBr_{3-x}$ after cooling. A template method was developed for analyzing the big data of *in situ* SAED movies, which successfully reveal detailed information of the phase evolution. δ-$CsPbI_xBr_{3-x}$ in the [001] zone axis converted to α-$CsPbI_xBr_{3-x}$ in the [011] zone axis in the *in situ* heating experiment. On this basis, a possible atom movement trajectory was proposed to recover the process of phase transition. It explains the increase of lattice volume during phase evolution, which could be caused by the unfolding of the Pb–X chain. The microstructure analysis provides a better understanding of the thermally driven phase evolution for halide perovskites. Moreover, the big data analysis based on the data dimension reduction and template method we have developed may be applied to other material systems including phase change, which is worth expecting.

IV. METHODS

A. Materials

For the TEM specimen preparation, $CsPbI_xBr_{3-x}$ nanowires synthesized by surfactant-free solution method, isopropanol [high-performance liquid chromatography (HPLC), 99.80%, from damas-beta], were used.

B. Transmission electron microscopy

TEM experiments were performed on the JEOL JEM-F200 microscope. An *in situ* heating holder (Protochips Fusion 350) was used to carry out *in situ* heating experiments. Images and diffraction data were obtained by a Gatan RIO 16 camera.

SUPPLEMENTARY MATERIAL

See the supplementary material for the *ex situ* morphology and SAED patterns of another nanowire in the *in situ* heating experiment; *ex situ* morphology and SAED patterns of another nanowire after cooling; the details of eigen-patterns and the weight of the two main principal components over time in PCA; and three movies showing the evolution of diffraction spots. The diffraction spots were labeled and colored by using the template matching method.

ACKNOWLEDGMENTS

This work was supported by the National Natural Science Foundation of China (Grant No. 52222311), the Double First-Class Initiative Fund of ShanghaiTech University, and the startup funding from ShanghaiTech University. The TEM characterization was supported by the Center for High-resolution Electron Microscopy (CℏEM) at ShanghaiTech University. The initiation of this project (nanowire synthesis and initial electron diffraction studies) was supported by the U.S. Department of Energy, Office of Science, Office of Basic Energy Sciences, Materials Sciences and Engineering Division, under Contract No. DE-AC02-05CH11231 within the Physical Chemistry of Inorganic Nanostructures Program (Grant No. KC3103).

AUTHOR DECLARATIONS

Conflict of Interest

The authors have no conflicts to disclose.

Author Contributions

The idea was proposed by Y.Y., P.Y., and X.L. T.L. synthesized $CsPbI_xBr_{3-x}$ nanowires. Initial TEM studies were started at Berkeley by Y.Y. and T.L. *In situ* heating TEM characterization was performed by X.L. and W.L. The big data processing based on data dimension reduction and template method was finished by X.L. Z.Y. contributed to the application of the PCA method for data processing.

Xin Luo: Conceptualization (equal); Data curation (lead); Investigation (lead); Methodology (lead); Writing – original draft (lead); Writing – review & editing (equal). **Weiyan Liu**: Data curation (equal); Investigation (equal). **Zeyu Wang**: Data curation (equal). **Teng Lei**: Data curation (equal). **Peidong Yang**: Conceptualization (lead); Funding acquisition (lead); Project administration (lead); Resources (lead); Supervision (equal); Writing – review & editing (lead). **Yi Yu**: Conceptualization (lead); Funding acquisition (lead); Methodology (lead); Project administration (lead); Resources (lead); Supervision (lead); Writing – original draft (lead); Writing – review & editing (lead).

DATA AVAILABILITY

The data that support the findings of this study are available from the corresponding authors upon reasonable request.

REFERENCES

[1]M. A. Green, A. Ho-Baillie, and H. J. Snaith, Nat. Photonics **8**(7), 506–514 (2014).

[2]S. D. Stranks and H. J. Snaith, Nat. Nanotechnol. **10**(5), 391–402 (2015).

[3]W. Zhang, G. E. Eperon, and H. J. Snaith, Nat. Energy **1**(6), 16048 (2016).

[4]M. Liu, M. B. Johnston, and H. J. Snaith, Nature **501**(7467), 395–398 (2013).

[5]A. Marronnier, G. Roma, S. Boyer-Richard, L. Pedesseau, J.-M. Jancu, Y. Bonnassieux, C. Katan, C. C. Stoumpos, M. G. Kanatzidis, and J. Even, ACS Nano **12**(4), 3477–3486 (2018).

[6]C. Yi, J. Luo, S. Meloni, A. Boziki, N. Ashari-Astani, C. Grätzel, S. M. Zakeeruddin, U. Röthlisberger, and M. Grätzel, Energy Environ. Sci. **9**(2), 656–662 (2016).

[7]J. A. Christians, S. N. Habisreutinger, J. J. Berry, and J. M. Luther, ACS Energy Lett. **3**(9), 2136–2143 (2018).

[8]R. J. Sutton, M. R. Filip, A. A. Haghighirad, N. Sakai, B. Wenger, F. Giustino, and H. J. Snaith, ACS Energy Lett. **3**(8), 1787–1794 (2018).

[9]S. Dastidar, C. J. Hawley, A. D. Dillon, A. D. Gutierrez-Perez, J. E. Spanier, and A. T. Fafarman, J. Phys. Chem. Lett. **8**(6), 1278–1282 (2017).

[10]C. K. Møller, *The Structure of Cæsium Plumbo Iodide $CsPbI_3$* (Munksgaard, 1959).

[11]D. B. Straus, S. Guo, and R. J. Cava, J. Am. Chem. Soc. **141**(29), 11435–11439 (2019).

[12]D. M. Trots and S. V. Myagkota, J. Phys. Chem. Solids **69**(10), 2520–2526 (2008).

[13]D. Zhang, S. W. Eaton, Y. Yu, L. Dou, and P. Yang, J. Am. Chem. Soc. **137**(29), 9230–9233 (2015).

[14]L. Dou, A. B. Wong, Y. Yu, M. Lai, N. Kornienko, S. W. Eaton, A. Fu, C. G. Bischak, J. Ma, and T. Ding, Science **349**(6255), 1518–1521 (2015).

[15]C. G. Bischak, M. Lai, Z. Fan, D. Lu, P. David, D. Dong, H. Chen, A. S. Etman, T. Lei, J. Sun, M. Grünwald, D. T. Limmer, P. Yang, and N. S. Ginsberg, Matter **3**(2), 534–545 (2020).

[16]C. L. Jia, M. Lentzen, and K. Urban, Science **299**(5608), 870–873 (2003).

[17]Y. Yu, D. Zhang, C. Kisielowski, L. Dou, N. Kornienko, Y. Bekenstein, A. B. Wong, A. P. Alivisatos, and P. Yang, Nano Lett. **16**(12), 7530–7535 (2016).

[18]M. Ge, F. Su, Z. Zhao, and D. Su, Mater. Today Nano **11**, 100087 (2020).

[19]J. Madsen, P. Liu, J. Kling, J. B. Wagner, T. W. Hansen, O. Winther, and J. Schiøtz, Adv. Theory Simul. **1**(8), 1800037 (2018).

[20]X. Luo, W. Liu, Z. Wang, C. Liang, X. He, and Y. Yu, ACS Appl. Energy Mater. **4**, 7226 (2021).

[21]Z. Lin, Y. Zhang, M. Gao, J. A. Steele, S. Louisia, S. Yu, L. N. Quan, C.-K. Lin, D. T. Limmer, and P. Yang, Matter **4**(7), 2392–2402 (2021).